

# THREE-PION INTERFEROMETRY OF RELATIVISTIC NUCLEAR COLLISIONS

Hiroki Nakamura<sup>(1)</sup> and Ryoichi Seki<sup>(2,3)</sup>

<sup>(1)</sup> *Department of Physics, Waseda University, Tokyo 169-8555, Japan*

<sup>(2)</sup> *Department of Physics, California State University, Northridge, CA 91330*

<sup>(3)</sup> *W. K. Kellogg Radiation Laboratory 106-38, California Institute of Technology, Pasadena, CA 91125*

(July 2, 2021)

## Abstract

Three-pion interferometry is investigated for new information on the space-time structure of the pion source created in ultra-relativistic heavy-ion collisions. The two- and three-pion correlations are numerically computed for incoherent source functions based on the Bjorken hydrodynamical model, over a wide range of the kinematic variables. New information provided by three-pion interferometry, different from that provided by two-pion interferometry, should appear in the phases of the Fourier transform of the source function. Variables are identified that would be sensitive to the phases and suitable for observation. For a positive, chaotic source function, however, a variation of the three-pion phase is found to be difficult to extract from experiments. Effects of asymmetry of the source function are also examined.

PACS number(s): 25.75 Gz

Typeset using REVTeX

## I. INTRODUCTION

Two-pion interferometry has been regarded as an important means of obtaining the space-time structure of dynamics involved in relativistic heavy-ion collisions. Over the years, extensive studies of two-pion interferometry have been carried out theoretically and experimentally to investigate how much information the correlations of two emitted pions can provide. As experiments become refined, measurements of three-pion correlations should become feasible, hopefully providing new information. The first result of such measurements has been recently reported from the CERN NA44 experiment [1].

In the last few years, some theoretical investigations have been made regarding three-pion interferometry [2,4–6]. Though the treatments of three-pion interferometry and the issues involved are similar to those regarding two-pion interferometry, three-pion interferometry is technically far more complicated than the two-pion case due to the involvement of an additional momentum and also to new aspects of the particle correlations. Consequently, theoretical work so far has been on limited aspects of the interferometry, focusing on a few kinematic variables, such as the sum of three relative invariant momenta, over small ranges of their values.

In the coming years, especially when RHIC becomes in operation, we expect that experiments on three-pion interferometry will become more detailed and will be made over larger ranges of various kinematic variables. We report here an investigation of three-pion interferometry over a wide range of kinematic variables. Our major objective is to clarify how much new information we can extract from three-pion interferometry, regarding the space-time structure of the pion source created in ultra-relativistic heavy-ion collisions. This work is similar to that of Heinz and Zhang [2] in its objective, but it differs in scope. We numerically calculate the two- and three-pion correlations for the same source functions and compare the two types of correlations. The calculations are carried out with various model source functions that are based on the Bjorken hydrodynamical model. Throughout this work, we assume pion emission from the source to be completely chaotic. We also neglect possible final-state interactions (including the Coulomb interactions) between the emitted pions and the source.

The new aspect of the correlations that three-pion interferometry can provide is the phase of the source function's Fourier transform. The information content of the phase differs from that of the magnitude of the Fourier transform. Since two-pion interferometry can provide only the magnitude, we hope that three-pion interferometry can provide new information. To this end, we carefully identify the variables that are sensitive to the phase and suitable for observation. Since the phase is expected to be greatly affected by asymmetry of the source function, we also examine that issue.

In Sec. II, we summarize the formulation of both the two- and the three-pion interferometries, mainly to define the correlation functions used. In Sec. III, we describe the various source functions that are used in the calculation, based on the Bjorken hydrodynamical model. The choice of optimal variables in the three-pion correlations is given in Sec. IV, and various numerical results are described in Sec. V. Discussion and conclusions are presented in Sec. VI.

## II. FORMALISM

The two- and three-particle correlation functions that we discuss are reasonably well-known, but for clarity we sketch the formalism of, in our case, bosons, and we define the correlation functions and various variables that appear in this work.

The field operator  $\varphi(x)$  of emitted bosons, such as pions and kaons, obeys the Klein-Gordon equation,

$$(\partial^2 + m^2)\varphi(x) = J(x), \quad (1)$$

where  $m$  is the mass of the particle, and  $J(x)$  the source current [8]. The incoming and outgoing states of  $\varphi(x)$  are specified in terms of the creation and annihilation operators  $a^\dagger$  and  $a$  for these states. They are related to  $J(x)$  as

$$a_{\text{out}}(\mathbf{p}) = a_{\text{in}}(\mathbf{p}) + i \int d^4x \frac{1}{\sqrt{(2\pi)^3 \cdot 2\omega_p}} J(x) e^{-ip \cdot x}, \quad (2)$$

where  $p_0$  is on-shell and  $\omega_p = \sqrt{\mathbf{p}^2 + m^2}$ .

We define an important quantity in this work, a source function,  $S(x, K)$ , in terms of  $J(x)$ :

$$S(x, K) = \int \langle J^\dagger(x + \frac{y}{2}) J(x - \frac{y}{2}) \rangle e^{iK \cdot y} d^4y, \quad (3)$$

where  $\langle \dots \rangle$  denotes the quantum ensemble average over various incoming states. The Fourier transform of  $S(x, K)$  is defined as [2]

$$\begin{aligned} \rho(q, K) &= \int S(x, K) e^{iq \cdot x} d^4x \\ &\equiv f(q, K) \exp(i\phi(q, K)). \end{aligned} \quad (4) \quad (5)$$

where  $f(q, K)$  is the amplitude and  $\phi(q, K)$  the phase. For a real  $S(x, K)$ , we have  $f(q, K) = f(-q, K)$  and  $\phi(q, K) = -\phi(-q, K)$ , and thus  $\phi(0, K) = 0$ . Boson spectra and correlation functions will be expressed in terms of  $\rho(q, K)$  or  $S(x, K)$ , and  $\phi(q, K)$  is written in the small-momentum expansion as [2]

$$\phi(q, K) = \langle x \rangle_K \cdot q - \frac{1}{6} \langle (q \cdot \tilde{x}_K)^3 \rangle_K + O(q^5), \quad (6)$$

where  $\langle \dots \rangle_K = \int S(x, K) \dots d^4x$ , and  $\tilde{x}_K = x - \langle x \rangle_K$ . Since  $\phi(q, K)$  is written in terms of odd moments of  $x$ , an asymmetric (about  $x$ ) source causes a strong, nonlinear dependence of  $\phi(q, K)$  on  $q$ . In this work, we examine the  $S(x, K)$  of simple forms as discussed in Sec. III.

The one-particle spectrum is given by

$$\begin{aligned} W_1(\mathbf{p}_1) &= \langle a_{\text{out}}^\dagger(\mathbf{p}_1) a_{\text{out}}(\mathbf{p}_1) \rangle \\ &= \frac{1}{(2\pi)^3 2\omega_{p_1}} \int S(x, p_1) d^4x \\ &= \frac{1}{(2\pi)^3 2\omega_{p_1}} f(0, p_1). \end{aligned} \quad (7)$$

Higher-order correlations of  $J(x)$  are assumed to satisfy Gaussian reduction, such as

$$\begin{aligned} & \langle J^\dagger(x_1)J^\dagger(x_2)J(y_1)J(y_2) \rangle = \\ & \langle J^\dagger(x_1)J(y_1) \rangle \langle J^\dagger(x_2)J(y_2) \rangle + \langle J^\dagger(x_1)J(y_2) \rangle \langle J^\dagger(x_2)J(y_1) \rangle. \end{aligned} \quad (8)$$

The two-particle spectrum is then written as

$$\begin{aligned} W_2(\mathbf{p}_1, \mathbf{p}_2) &= \langle a_{\text{out}}^\dagger(\mathbf{p}_1)a_{\text{out}}(\mathbf{p}_1)a_{\text{out}}^\dagger(\mathbf{p}_2)a_{\text{out}}(\mathbf{p}_2) \rangle \\ &= W_1(\mathbf{p}_1)W_1(\mathbf{p}_2) + \frac{1}{(2\pi)^6 \cdot 2\omega_{p_1} \cdot 2\omega_{p_2}} \left| \int S(x, K_{12}) e^{iq_{12} \cdot x} d^4x \right|^2 \\ &= W_1(\mathbf{p}_1)W_1(\mathbf{p}_2) + \frac{1}{(2\pi)^6 \cdot 2\omega_{p_1} \cdot 2\omega_{p_2}} f^2(q_{12}, K_{12}), \end{aligned} \quad (9)$$

where for the pair of the  $i$ -th and  $j$ -th momenta, we define their average and relative momenta as

$$\begin{aligned} K_{ij} &= \frac{p_i + p_j}{2}, \\ q_{ij} &= p_i - p_j, \end{aligned} \quad (10)$$

respectively. The two-particle correlation function is then expressed as

$$\begin{aligned} C_2(\mathbf{p}_1, \mathbf{p}_2) &= \frac{W_2(\mathbf{p}_1, \mathbf{p}_2)}{W_1(\mathbf{p}_1)W_1(\mathbf{p}_2)} \\ &= 1 + \frac{f_{12}^2}{f_{11}f_{22}}. \end{aligned} \quad (11)$$

Hereafter, we denote  $f_{ij}$  for  $f(q_{ij}, K_{ij})$  and  $\phi_{ij}$  for  $\phi(q_{ij}, K_{ij})$ . Equation (11) shows that the two-particle correlation function is independent of  $\phi_{ij}$ .

Similarly, the three-particle spectrum and correlation are given by

$$W_3(\mathbf{p}_1, \mathbf{p}_2, \mathbf{p}_3) = \langle a_{\text{out}}^\dagger(\mathbf{p}_1)a_{\text{out}}(\mathbf{p}_1)a_{\text{out}}^\dagger(\mathbf{p}_2)a_{\text{out}}(\mathbf{p}_2)a_{\text{out}}^\dagger(\mathbf{p}_3)a_{\text{out}}(\mathbf{p}_3) \rangle, \quad (12)$$

and

$$\begin{aligned} C_3(\mathbf{p}_1, \mathbf{p}_2, \mathbf{p}_3) &= \frac{W_3(\mathbf{p}_1, \mathbf{p}_2, \mathbf{p}_3)}{W_1(\mathbf{p}_1)W_1(\mathbf{p}_2)W_1(\mathbf{p}_3)} \\ &= 1 + \frac{f_{12}^2}{f_{11}f_{22}} + \frac{f_{23}^2}{f_{22}f_{33}} + \frac{f_{31}^2}{f_{33}f_{11}} \\ &\quad + 2F_3 \cos \Phi, \end{aligned} \quad (13)$$

where

$$\begin{aligned} \Phi &= \phi_{12} + \phi_{23} + \phi_{31} \\ F_3 &= \frac{f_{12}f_{23}f_{31}}{f_{11}f_{22}f_{33}}. \end{aligned} \quad (14)$$

From the preceding discussion of  $\phi_{ij}$ , we have

$$\Phi(p_1 = p_2 = p_3) = 0 \quad (15)$$

for a real source function. When  $\langle x \rangle_{K_{12}} \approx \langle x \rangle_{K_{23}} \approx \langle x \rangle_{K_{31}}$ , Eq. (6) yields

$$\Phi \approx -\frac{1}{6} \left[ \langle (q_{12} \cdot \tilde{x}_{K_{12}})^3 \rangle_{K_{12}} + \langle (q_{23} \cdot \tilde{x}_{K_{23}})^3 \rangle_{K_{23}} + \langle (q_{31} \cdot \tilde{x}_{K_{31}})^3 \rangle_{K_{31}} \right]; \quad (16)$$

$\Phi$  is thus expected to vary prominently when the source is asymmetric (in  $x$ ).

Equation (13) shows that the three-particle correlation function depends on  $\cos \Phi$ , which is absent in the two-particle correlation. The rest of the three-particle correlation is expressed in terms of  $f_{ij}$ 's and can thus be determined from the two-particle correlations.

The three-particle correlation is a function of three momenta,  $\mathbf{p}_1$ ,  $\mathbf{p}_2$ , and  $\mathbf{p}_3$ . For convenience, we introduce the average total momentum,

$$K = \frac{p_1 + p_2 + p_3}{3}. \quad (17)$$

Since  $q_{ij}$ 's satisfy the identity,

$$q_{12} + q_{23} + q_{31} = 0, \quad (18)$$

we have three independent momentum variables, which we will take to be  $K$ ,  $q_{12}$ , and  $q_{23}$ .

Among various choices of three variables, another convenient choice is a set of  $K_{ij}$ 's. For completeness, we show the relations between the first set and  $K_{ij}$ 's:

$$K_{12} = K + \frac{1}{6}(q_{23} - q_{31}), \quad K_{23} = K + \frac{1}{6}(q_{31} - q_{12}), \quad K_{31} = K + \frac{1}{6}(q_{12} - q_{23}), \quad (19)$$

satisfying

$$K = \frac{K_{12} + K_{23} + K_{31}}{3}. \quad (20)$$

### III. SOURCE FUNCTION

We apply the Bjorken hydrodynamical model to describe the evolution of the hot region created in heavy-ion collisions. Based on the Cooper-Frye spectrum, one writes the source function as [3]

$$\begin{aligned} S(x, K) d^4x &= F(\tau, \eta) d\tau \exp\left(-\frac{\mathbf{x}_T^2}{2R_T^2}\right) \times K \cdot d\sigma \exp\left(-\frac{K \cdot U}{T_f}\right) \\ &= F(\tau, \eta) d\tau \exp\left(-\frac{\mathbf{x}_T^2}{2R_T^2}\right) \times m_T \cosh(Y - \eta) e^{-\frac{m_T}{T_f} \cosh(Y - \eta)} \tau d\eta d^2\mathbf{x}_T, \end{aligned} \quad (21)$$

where  $\tau$ ,  $\eta$ , and  $\mathbf{x}_T$  denote the coordinate variables defined as  $\tau = \sqrt{t^2 - z^2}$ ,  $\eta = \frac{1}{2} \log\left(\frac{t+z}{t-z}\right)$ , and  $\mathbf{x}_T = (x, y)$ , respectively;  $m_T$  and  $Y$  are the momentum variables defined as  $m_T = \sqrt{K_0^2 - K_z^2}$  and  $Y = \frac{1}{2} \log\left(\frac{K_0 + K_z}{K_0 - K_z}\right)$ , respectively. Note that we specify the momentum

variables for a momentum pair,  $p_i$  and  $p_j$ , by the subscript  $ij$ , such as  $m_{Tij}$ , and those for three momenta with no subscript such as  $m_T$ . We set the  $z$ -axis to be the beam direction, and the  $x$ -axis parallel to  $\mathbf{K}_T$ , or perpendicular to the beam axis.  $U^\mu$  is a four-velocity of flow, and is  $U^\mu = (\frac{t}{\tau}, 0, 0, \frac{z}{\tau})$  in the Bjorken hydrodynamical model. The profile function  $F(\tau, \eta)$  determines the source shape in the  $\tau$ - $\eta$  space. The shape along the transverse direction is taken to be of a Gaussian form.  $T_f$  is the freeze-out temperature, and  $d\sigma_\mu$  is the measure of freeze-out hypersurface. We assume that freeze-out occurs on the hypersurface where  $\tau$  is constant.

In this work, we examine the following five forms of the profile function. Simple (box-type) profile:

$$F(\tau, \eta) = \begin{cases} \delta(\tau - \tau_0) & (|\eta| < \Delta\eta) \\ 0 & (\text{otherwise}) \end{cases} \quad (22)$$

Gaussian profile:

$$F(\tau, \eta) = \delta(\tau - \tau_0) \exp\left(-\frac{\eta^2}{2\Delta\eta^2}\right) \quad (23)$$

Heinz profile:

$$F(\tau, \eta) = \frac{1}{(2\pi)\Delta\tau} \exp\left(-\frac{(\tau - \tau_0)^2}{2\Delta\tau^2} - \frac{\eta^2}{2\Delta\eta^2}\right) \quad (24)$$

Exponential profile:

$$F(\tau, \eta) = \frac{1}{\Delta\tau} \theta(\tau - \tau_0) \exp\left(-\frac{\tau - \tau_0}{\Delta\tau} - \frac{\eta^2}{2\Delta\eta^2}\right) \quad (25)$$

Theta profile:

$$F(\tau, \eta) = \frac{1}{(\pi)\Delta\tau} \theta(\tau - \tau_0) \exp\left(-\frac{(\tau - \tau_0)^2}{2\Delta\tau^2} - \frac{\eta^2}{2\Delta\eta^2}\right) \quad (26)$$

#### IV. OPTIMAL VARIABLES

The three-particle correlation function depends on three momenta, which have nine components. As noted in Sec. II, we choose the three momenta to be  $K$ ,  $q_{12}$ , and  $q_{23}$ . In this work, we focus on the dependence of the correlation functions on relative momenta of the emitted bosons by fixing the value of  $K$ . This leaves the two relative momenta to be the remaining variables.

In order to identify new information in the correlation function, we should choose the variables that could provide the most rapid variation of  $\cos\Phi$ . Figure 1 illustrates the variation of  $\cos\Phi$  as a function of  $q_{12}^z$  and  $q_{23}^z$  with all other components of the relative momenta set to be zero. Here, we use the Heinz profile with the parameters of  $\tau_0 = 6$  fm,  $\Delta\tau = 1$  fm,  $\Delta\eta = 1.2$ , and  $m_T = T_f = 140$  MeV. Figure 1 shows that  $\cos\Phi$  is unity along

the  $q_{12}^z$ - and  $q_{23}^z$ -axes and also along the line of  $q_{12}^z = -q_{23}^z$ , or the  $q_{31}^z$ -axis (because of Eq. (16)). Figure 1 also shows that  $\cos \Phi$  varies most prominently along the lines of  $q_{12}^z = q_{23}^z$ ,  $q_{23}^z = q_{31}^z$ , and  $q_{31}^z = q_{12}^z$ . Because of symmetry, however, it is sufficient to examine the variation around one of the lines, such as the line of  $q_{12}^z = q_{23}^z$ .

The reason why the line of  $q_{12}^z = q_{23}^z$  provides a prominent variation of  $\cos \Phi$  is seen as follows. When  $q_{ij} \ll K_{ij}$  and  $K_{12} \approx K_{23} \approx K_{31}$ , we have

$$\Phi \approx \phi(q_{12}) + \phi(q_{23}) + \phi(-q_{12} - q_{23}), \quad (27)$$

where the (weak) dependence on  $K_{ij}$  in  $\phi$  is not explicitly shown. Setting  $q_{12}^z = q_z \cos \theta$  and  $q_{23}^z = q_z \sin \theta$ , we find

$$\begin{aligned} \frac{\partial \Phi}{\partial \theta} \approx & -q_z \sin \theta \phi'(q_{12}^x, q_{12}^y, q_z \cos \theta) + q_z \cos \theta \phi'(q_{23}^x, q_{23}^y, q_z \sin \theta) \\ & - q_z (\cos \theta - \sin \theta) \phi'(-q_{12}^x - q_{23}^x, -q_{12}^y - q_{23}^y, -q_z (\cos \theta + \sin \theta)), \end{aligned} \quad (28)$$

where  $\phi'(\mathbf{q}) = \partial \phi / \partial q_z$ . When  $q_{12}^x = q_{23}^x$  and  $q_{12}^y = q_{23}^y$ ,  $\partial \Phi / \partial \theta$  vanishes at  $\theta = \pi/4$ , or  $q_{12}^z = q_{23}^z$ , yielding the minimum. It follows then that the optimum choice is  $q_{12} = q_{23}$ .

With this constraint, the variables are now reduced to a single relative momentum.

The source functions under consideration (as listed in Sec. III) are almost symmetric about the beam and transverse axes, but they can be asymmetric about the time-axis. Which component of  $q_{12}$  ( $= q_{23}$ ) should we choose so as to describe most effectively the asymmetric property of the source functions?  $q_{12}^0$  is an obvious choice, but we find that  $q_{12}^z$  or  $q_{12}^x$  is the most convenient variable. From Eq. (10), we have  $K_{12} \cdot q_{12} = 0$ , which gives  $q_{12} \cdot x = q_{12}^z (tK_{12}^z / K_{12}^0 - z) + q_{12}^x (tK_{12}^T / K_{12}^0 - x) - q_{12}^y y$ . Thus  $\cos \Phi$  as a function of  $q_{12}^z$  or  $q_{12}^x$  reflects time-axis asymmetry. Furthermore, for finite  $Y_{12}$ , our source functions are not simply a function of  $z^2$  without symmetry along the longitudinal direction. Because of this,  $q_{12}^x$  may be the variable more suitable for identifying the time-axis asymmetry of the source function. In the following, we will examine both  $q_{12}^z$  and  $q_{12}^x$ .

$q_{12}^x$  is parallel to  $\mathbf{K}_{12}^T$ , while  $q_{12}^y$  is perpendicular to it. Following the practice in the literature on two-pion interferometry, we will also denote  $q_{12}^x$  and  $q_{12}^y$  as  $q_{\text{out}}$  and  $q_{\text{side}}$ , respectively. Note that when the dependence of  $\cos \Phi$  on  $q_{12}^z$  or  $q_{12}^x$  is examined, the other components of  $q_{12}$  are fixed in our calculation.

## V. NUMERICAL RESULTS

Figures 2, 4, 6, 8, and 10 illustrate the dependence of  $f_{12}$  and  $\phi_{12}$  on  $q_{12}^z$  in the Heinz, Simple, Gaussian, Theta, and Exponential profile functions, respectively. Each figure is shown for  $Y_{12} = 0, 1$ , and 2. In the figures, we set  $q_{12}^{\text{out}} = q_{12}^{\text{side}} = 0$ ,  $m_{T12} = 140$  MeV,  $T_f = 140$  MeV,  $\Delta\eta = 1.2$ , and  $\tau_0 = 6$  fm for all profile functions, and also  $\Delta\tau = 1$  fm for the Heinz, Theta, and Exponential profile functions. These parameter values reasonably satisfy the recent CERN-SPS experiment on Pb + Pb at 158 GeV/A [7]. Note that  $|f_{12}|^2 + 1$  describes the two-particle correlation since  $f_{12}$  is normalized to be unity at  $q_{12}^z = 0$ , and that  $\phi$  is not observed in the experiment.

Figures 3, 5, 7, 9, and 11 show  $\cos \Phi$  and (half of) its coefficient in the three-particle correlation function,  $F_3$ , as functions of  $q_z$  ( $\equiv q_{12}^z = q_{23}^z$ ). Each figure is shown for  $Y = 0, 1$ ,

and 2 and  $m_T = 140$  MeV with the parameter values of  $T_f$ ,  $\Delta\eta$ ,  $\tau_0$ , and  $\Delta\tau$  as in Figs. 2, 4, 6, 8, and 10.

In Figs. 3, 5, 7, 9, and 11, we see that for all profile functions,  $\cos\Phi = 1$  at  $Y = 0$ , and  $\cos\Phi$  becomes more prominent as  $Y$  increases.  $\cos\Phi$  tends to be smaller for the asymmetric profile functions (such as the Simple and Exponential profile functions) than for the symmetric ones, though the difference between them is not substantial.  $\Phi$  tends to deviate from zero more slowly than the phases of  $\rho_{ij}$ 's,  $\phi_{ij}$ 's. For example, we see in Figs. 4 and 5 that when  $\phi_{12}$  reaches  $\pi/2$  around  $q_{12}^z = 150$  MeV, we still have  $\cos\Phi > 0.5$ . The reason for this is general because  $\Phi$  is defined as  $\Phi = \phi_{12} + \phi_{23} + \phi_{31}$  and is constrained by the identity,  $q_{12} + q_{23} + q_{31} = 0$ . In fact, the small-momentum expansion of Eq. (6) applied to  $\Phi$  yields that the term linear in  $q$  vanishes, as discussed in Sec. II. Furthermore, when  $\Phi$  starts to deviate from zero, its coefficient in the three-particle correlation function,  $2F_3$ , tends to become small. In fact, we see in the figures that  $2F_3$  gets halved for all profile functions before  $\cos\Phi$  decreases to 0.9, and even nearly vanishes when  $\cos\Phi$  decreases further. We expect that in actual experiments it will be difficult to identify  $\cos\Phi$  with a value much smaller than unity. This is the major finding of this work.

We find the same difficulty when we choose  $q_{\text{out}}$  as the independent variable. Figure 12 shows  $f_{12}$  and  $\phi_{12}$  as functions of  $q_{12}^{\text{out}}$  for the Heinz profile for  $m_{T12} = 140, 200, \text{ and } 300$  MeV, with  $\tau_0 = 6$  fm,  $Y_{12} = 1.5$ ,  $\Delta\eta = 1.2$ ,  $\Delta\tau = 1$  fm, and  $R_T = 5$  fm. Figure 13 also shows  $\cos\Phi$  and  $F_3$  as functions of  $q_{\text{out}} (= q_{12}^{\text{out}} = q_{23}^{\text{out}})$  for the three values of  $m_T$  with  $Y = 1.5$  and the same values of  $T_f$ ,  $\Delta\eta$ ,  $\Delta\tau$ ,  $\tau_0$ , and  $R_T$ . We see in Fig. 13 that when  $\cos\Phi$  starts to deviate from unity, its coefficient,  $2F_3$ , becomes small quite rapidly, as in the previous cases of  $q_{12}^z$  being the independent variable. Note that  $F_3$  decreases more quickly as a function of  $q_{\text{out}}$  than of  $q_z$ , as seen in Figs. 13 and 3. The quick reduction occurs because of the factor  $\exp\left(-\frac{x_T^2}{2R_T^2}\right)$ , when the transverse momentum,  $q_{\text{out}}$ , is used as the variable.  $R_T = 5$  fm is chosen to reproduce experimental results, but we find that even if a much smaller value of  $R_T$  is used,  $F_3$  becomes quite small when  $\cos\Phi$  is off unity.

The difficulty also remains at different values of  $\tau_0$ . Figures 14 and 15 show  $f_{12}$ ,  $\phi_{12}$ ,  $\cos\Phi$ , and  $F_3$  as functions of  $q_{12}^z$  for  $(\tau_0, \Delta\tau) = (6.5, 0.65), (4, 8, 2.8), \text{ and } (3.2, 3.2)$  fm, with  $m_T = m_{T12} = 140$  MeV,  $T_f = 140$  MeV,  $Y = Y_{12} = 1.5$ , and  $\Delta\eta = 1.2$ . These parameter sets yield the recently measured value of the longitudinal size,  $R_{\text{long}} = 3.5$  fm [7]. Figure 15 shows that  $\cos\Phi$  depends on  $\tau_0$  rather strongly. But the variation of  $\cos\Phi$  takes place where  $F_3$  is small, and will be difficult to observe.

## VI. DISCUSSIONS AND SUMMARY

We have investigated the three-particle correlation function for chaotic source, using various profile functions of the source in the Bjorken hydrodynamical model. In all profile functions we have examined, the coefficient of  $\cos\Phi$  in the three-particle correlation function,  $2F_3$ , decreases quite rapidly, as  $\cos\Phi$  decreases from unity. Extraction of  $\cos\Phi$  is thus difficult when  $\cos\Phi$  decreases from unity. This result is in agreement with Heinz and Zhang [2], who previously made a similar investigation for small relative momenta.

In order to clarify why  $\cos\Phi$  is difficult to observe, we first identify the portion of the source function  $S(x)$  that most strongly influences the phase,  $\phi$ .  $\phi$  appears in the Fourier



transform of  $S(x)$  as  $\rho(q) = \rho_R(q) + i\rho_I(q) = fe^{i\phi}$ . As noted previously,  $\phi$  is an odd function of  $q$ , and  $\phi(q=0) = 0$  for a real source function. The imaginary part of  $\rho(q)$ ,  $\rho_I(q)$ , thus represents the behavior of  $\phi$  relevant to the present discussion and is an odd function of  $q$ . The portion of  $S(x)$  that most strongly affects  $\phi$  is thus its odd-function part,  $S_{odd}(x)$ , in  $S(x) = S_{even}(x) + S_{odd}(x)$  with  $S_{odd}(-x) = -S_{odd}(x)$  and  $S_{even}(-x) = S_{even}(x)$ .

Consider that  $S_{even}(x)$  and  $S_{odd}(x)$  vary over distances of typical scale,  $\delta x_{even}$  and  $\delta x_{odd}$ , respectively. Here,  $\delta x_{even}$  and  $\delta x_{odd}$  correspond to the spread widths of  $S_{even}(x)$  and the distance to maximum of  $S_{odd}(x)$ , respectively, as Fig. 16 illustrates.  $\rho_R(q)$  and  $\rho_I(q)$  also vary over the scales of  $\delta x_{even}^{-1}$  and  $\delta x_{odd}^{-1}$ , respectively. As  $\phi$  increases,  $\rho_I(q)$  increases. The region where  $\rho_I(q)$  is appreciable is  $q > \delta x_{odd}^{-1}$ . The amplitude  $f$  becomes small in the region where  $q$  is larger than  $\delta x_{even}^{-1}$ .

Thus, if  $\delta x_{odd}^{-1} < \delta x_{even}^{-1}$ , the variation of  $\phi$  is not difficult to observe. This is, however, untenable as long as  $S(x)$  is positive everywhere. Consider  $S_{odd}(x) < 0$  in some region: we then have  $S_{even}(x) > |S_{odd}(x)|$  in that region, and furthermore,  $\delta x_{even} > \delta x_{odd}$ . The last inequality contradicts the desired inequality.

In this discussion, we have assumed the source function,  $S(x, K)$ , to be positive everywhere, as done in common practice. How realistic is this assumption? If  $S(x, K)$  is a statistical phase-space distribution,  $S(x, K)$  should not be negative everywhere. Generally speaking, however,  $S(x, K)$  can be locally negative, provided its integrals over  $x$  or  $K$  be positive. This property is similar to, for example, that of the Wigner function. Furthermore,  $S(x, K)$  that is locally negative suggests that it would be associated with some dynamics involving quantum correlation. This aspect of the interferometry is currently under investigation.

Measurement of the three-pion correlations from the CERN NA44 experiment has been recently reported [1] for the total relative momentum of up to about 300 MeV, and the extraction of  $\cos \Phi$  up to about 60 MeV. This total relative momentum is too small to observe the variation of  $\cos \Phi$  that is examined in this work. Taken as a constant,  $\cos \Phi$  is found to be about 0.2 [1] and is much smaller than the value of unity for a chaotic source, as discussed in this work. The reason for the small value is unknown, but it may be because of partial coherence of the source, or even because of a more exotic reason [10].

In summary, we have investigated three-particle interferometry from chaotic sources using the Bjorken hydrodynamical model. The optimal variables are identified suitable for extracting new information through the phase of the source function's Fourier transform. The three-particle correlations are calculated over a wide range of the kinematic variables. A variation of the three-pion phase is found to be difficult to observe experimentally because its coefficient, as it appears in the three-particle correlation function, becomes small in that region. This is the case if the source function is positive everywhere as conventionally assumed, and suggests the interesting possibility of the source function being locally negative.

## ACKNOWLEDGMENTS

We acknowledge M. C. Chu for his valuable contribution at the initial stage of this work. This research is partially supported by the U.S. National Science Foundation under grants

PHY88-17296 and PHY90-13248 at Caltech, and the U.S. Department of Energy under grant DE-FG03-87ER40347 at CSUN.

## REFERENCES

- [1] A. Sakaguchi *et al.* (NA44 collaboration), Nucl. Phys **A638**, 103c (1998); J. Schmidt-Sørensen *et al.* (NA44 collaboration), *ibid.*, 471c (1998); H. Bøggild *et al.* (NA44 Collaboration), Phys. Lett. B**455**, 77 (1999).
- [2] U. Heinz and Q. H. Zhang, Phys. Rev. C**56**, 426 (1997).
- [3] U. Heinz, Nucl. Phys. **A610**, 264c (1996).
- [4] J. G. Cramer and K. Kadija, Phys. Rev. C**53**, 908 (1996).
- [5] H. Heiselberg and A. P. Vischer, Phys. Rev. C**55**, 874 (1997).
- [6] T. J. Humanic, Phys. Rev. C**60**, 014901 (1999).
- [7] R. Ganz *et al.* (NA49 collaboration), nucl-ex/9808006.
- [8] We follow the conventions of J. D. Bjorken and S. D. Drell, as in their book, *Relativistic Fields* (McGraw Hill, N. Y., 1964): Four-vectors are denoted in regular letters and three vectors in bold letters, and the square of the four-momentum of a physical particle is the square of its mass.
- [9] J. D. Bjorken, Phys. Rev. D**17**, 140 (1983).
- [10] H. Nakamura and R. Seki, Caltech Kellogg preprint (1999).

## FIGURES

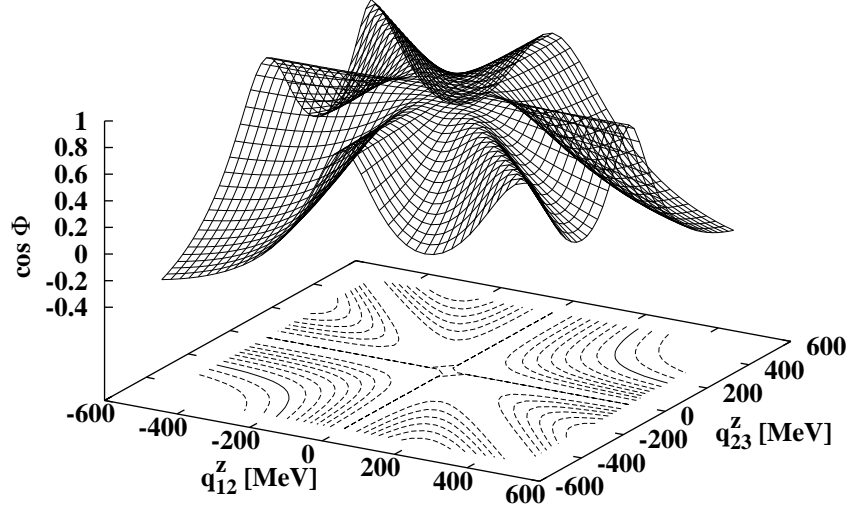


FIG. 1.  $\cos \Phi$  as a function of  $q_{12}^z$  and  $q_{23}^z$  for the Heinz profile function. The contour curves on the  $q_{12}^z - q_{23}^z$  plane are shown for the value of  $\cos \Phi$  from 0 to 1 by the step of 0.1. See the text for the parameter values used.

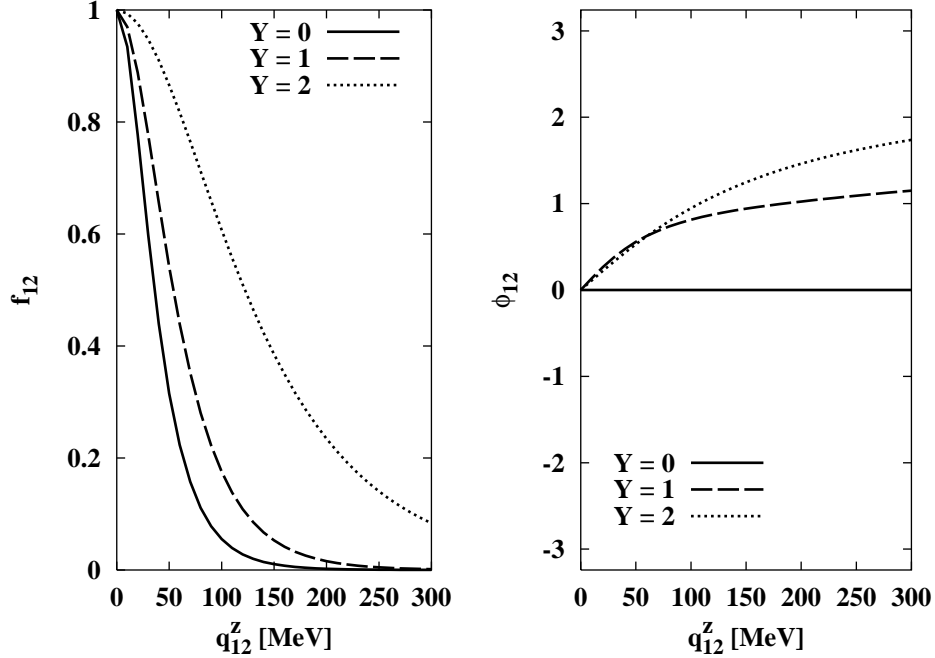


FIG. 2.  $f_{12}$  and  $\phi_{12}$  as functions of  $q_{12}^z$  for  $Y_{12} = 0, 1,$  and  $2$  in the Heinz profile function. See the text for the parameter values used.

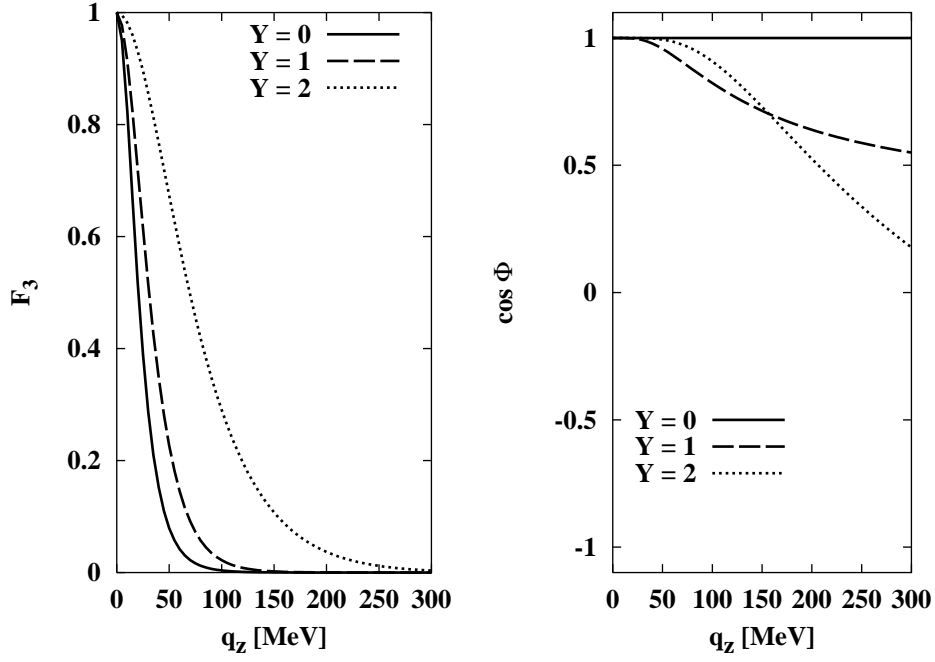


FIG. 3.  $\cos \Phi$  and  $F_3$  as functions of  $q_z$  with  $Y = 0, 1$ , and 2 for the Heinz profile function. See the text for the parameter values used.

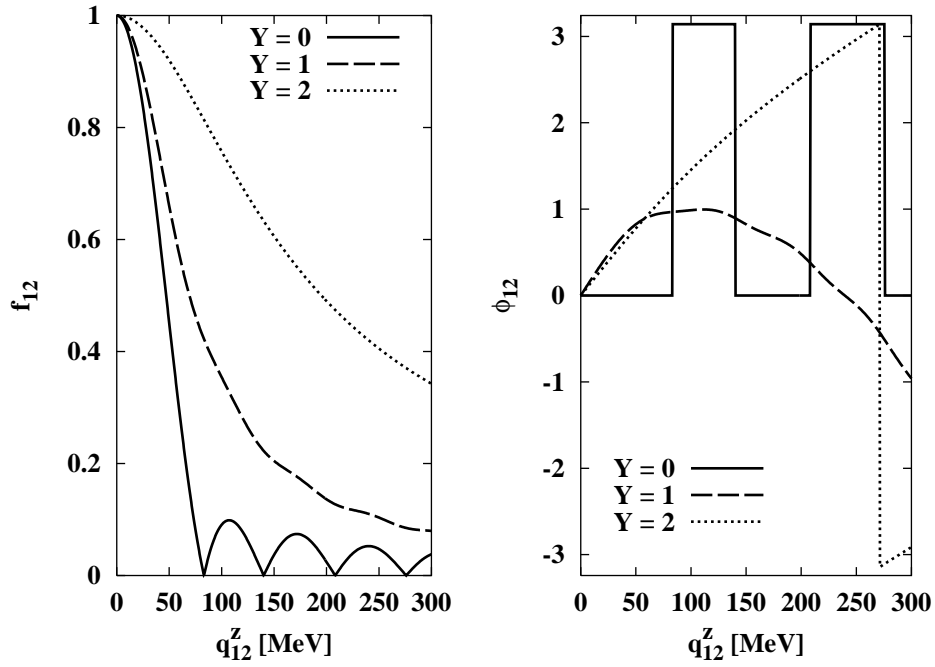


FIG. 4.  $f_{12}$  and  $\phi_{12}$  as functions of  $q_{12}^z$  with  $Y_{12} = 0, 1$ , and 2 for the Simple profile function. See the text for the parameter values used.

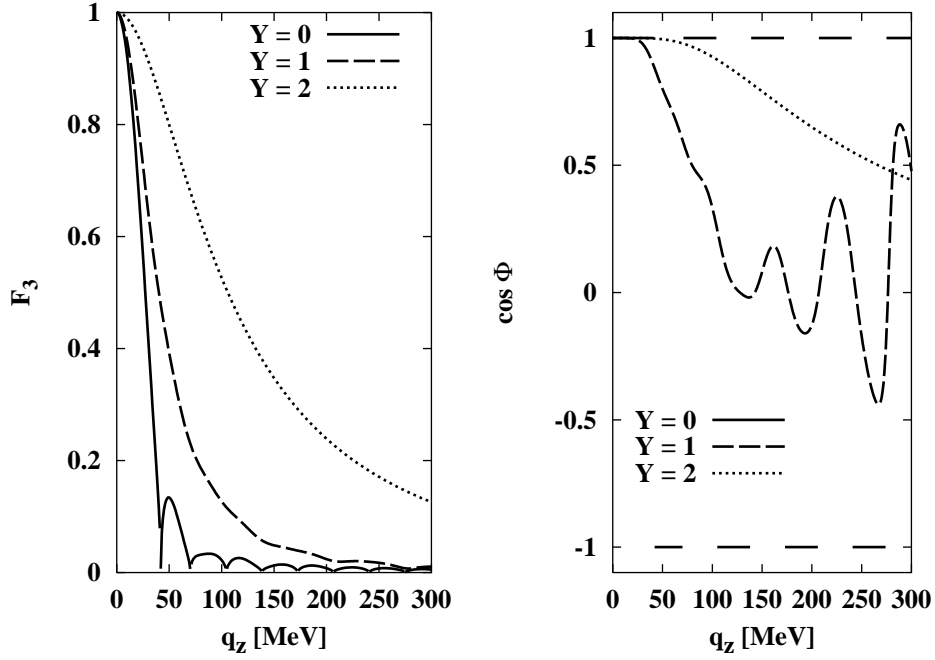


FIG. 5.  $\cos \Phi$  and  $F_3$  as functions of  $q_z$  with  $Y = 0, 1$ , and  $2$  in the Simple profile function. See the text for the parameter values used.

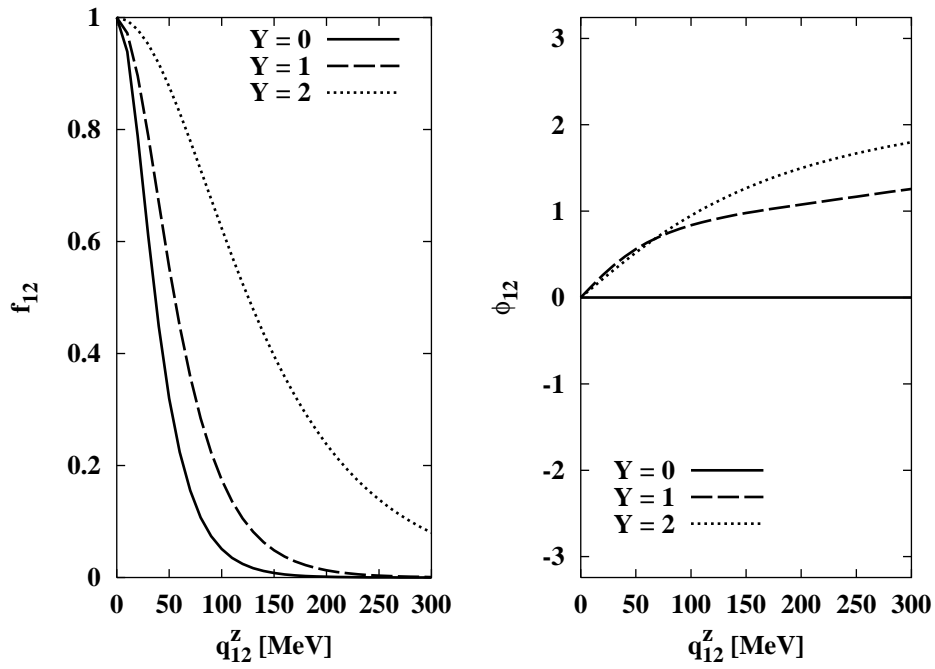


FIG. 6.  $f_{12}$  and  $\phi_{12}$  as functions of  $q_{12}^z$  with  $Y_{12} = 0, 1$ , and  $2$  in the Gaussian profile function. See the text for the parameter values used.

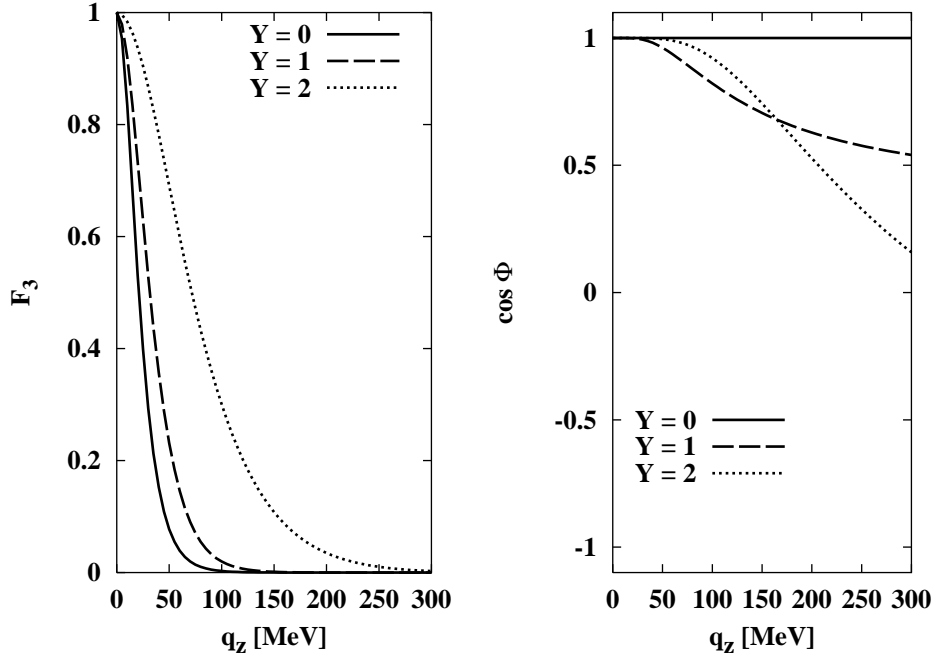


FIG. 7.  $\cos \Phi$  and  $F_3$  as functions of  $q_z$  for  $Y = 0, 1$ , and 2 in the Gaussian profile function. See the text for the parameter values used.

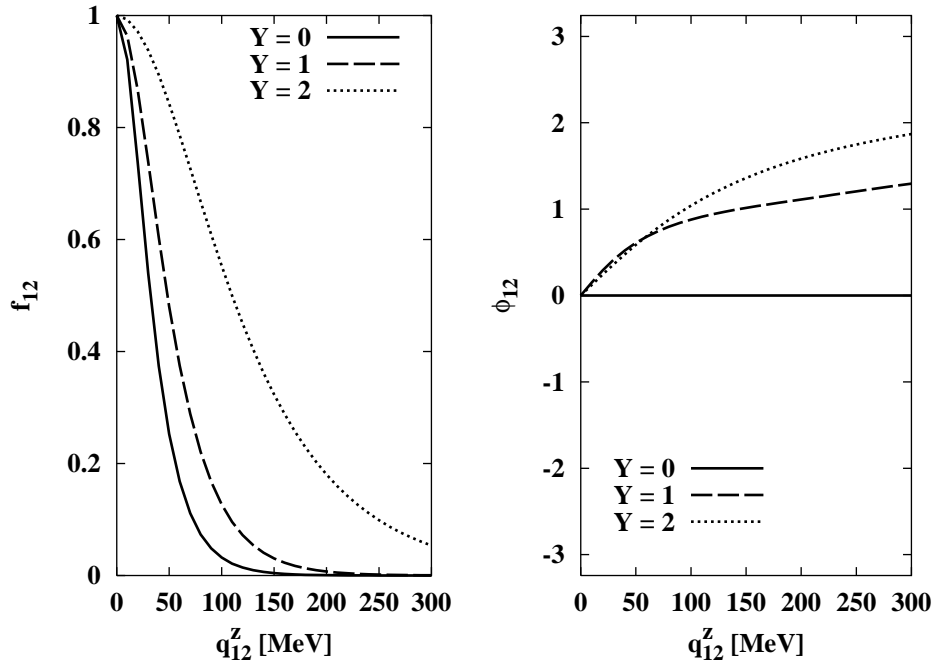


FIG. 8.  $f_{12}$  and  $\phi_{12}$  as functions of  $q_{12}^z$  for  $Y_{12} = 0, 1$ , and 2 in the Theta profile function. See the text for the parameter values used.

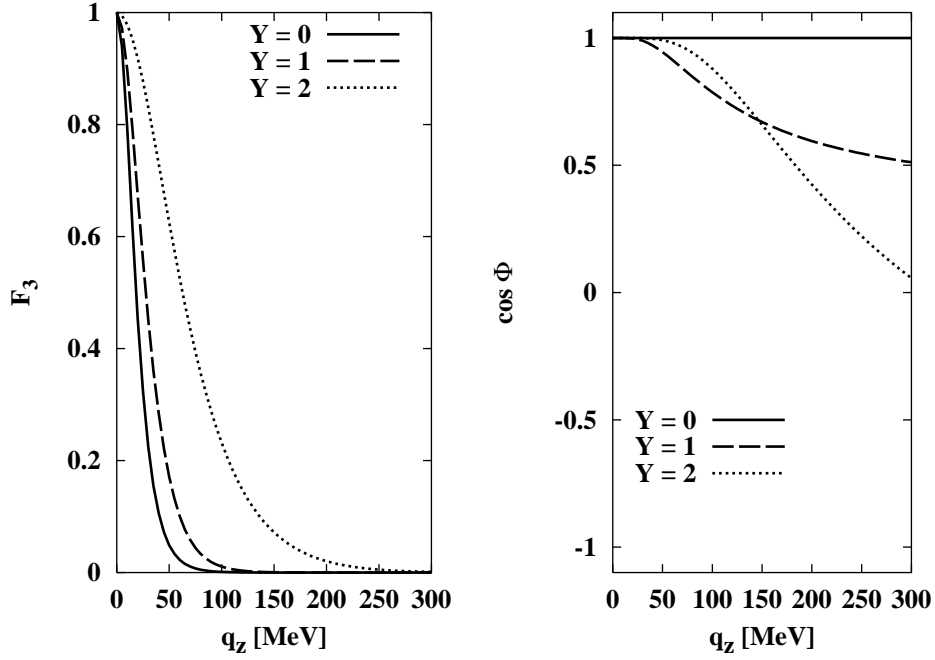


FIG. 9.  $\cos \Phi$  and  $F_3$  as functions of  $q_z$  for  $Y = 0, 1$ , and  $2$  in the Theta profile function. See the text for the parameter values used.

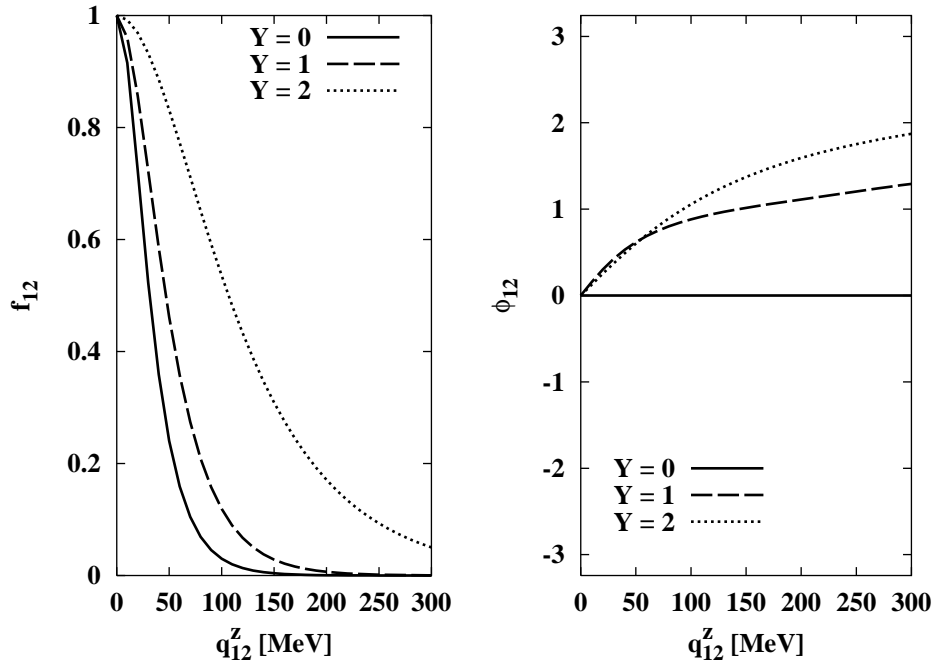


FIG. 10.  $f_{12}$  and  $\phi_{12}$  as functions of  $q_{12}^z$  for  $Y_{12} = 0, 1$ , and  $2$  in the Exponential profile function. See the text for the parameter values used.



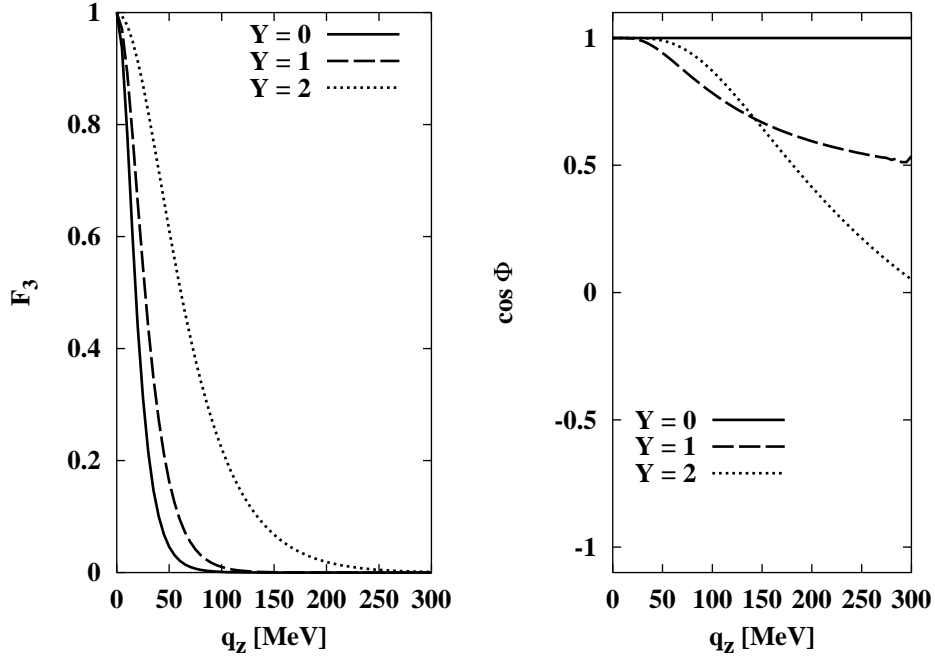


FIG. 11.  $\cos \Phi$  and  $F_3$  as functions of  $q_z$  for  $Y = 0, 1$ , and  $2$  in the Exponential profile function. See the text for the parameter values used.

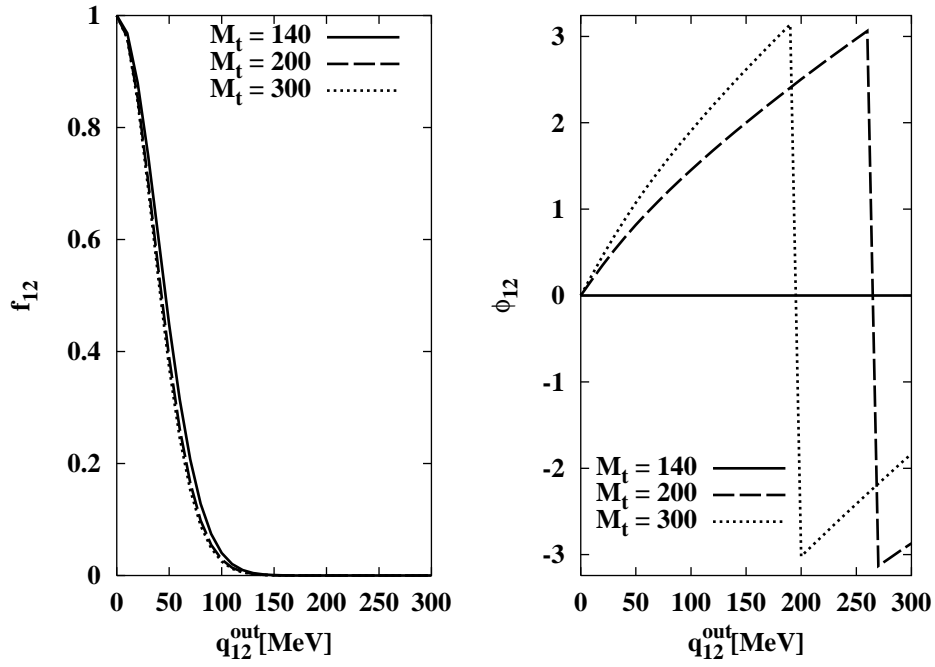


FIG. 12.  $f_{12}$  and  $\phi_{12}$  as functions of  $q_{12}^{out}$  for  $m_{T12} = 140, 200$ , and  $300$  MeV in the Heinz profile function. See the text for the parameter values used.

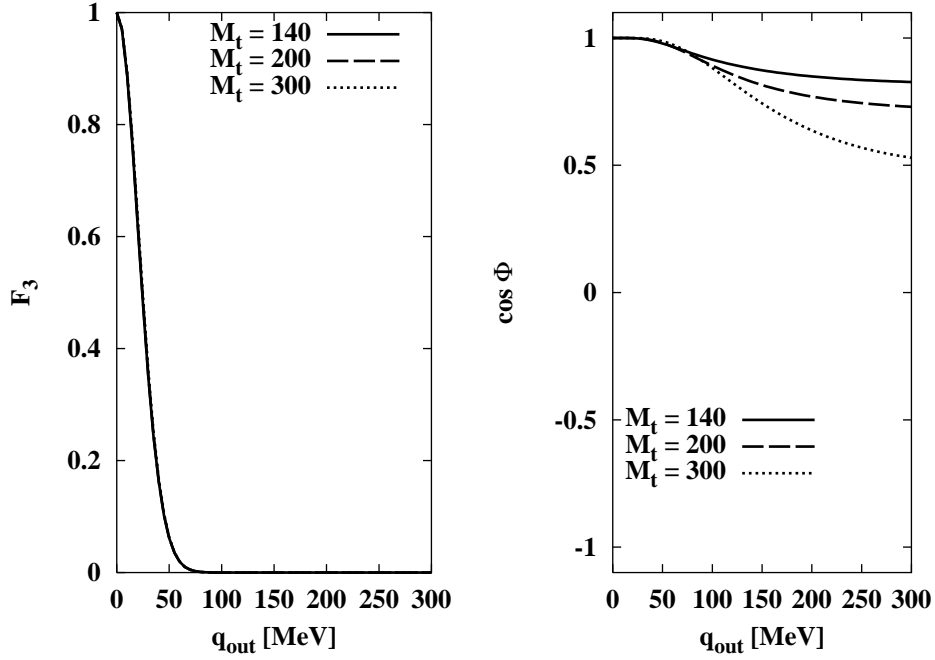


FIG. 13.  $\cos \Phi$  and  $F_3$  as functions of  $q_{\text{out}}$  for  $m_T = 140, 200,$  and  $300$  MeV in the Heinz profile function. See the text for the parameter values used.

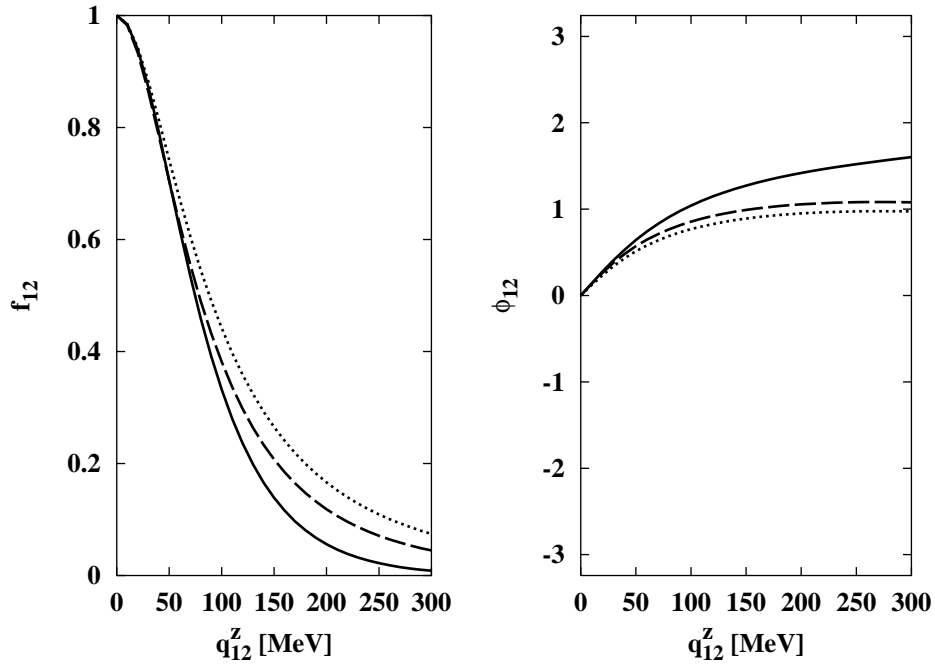


FIG. 14.  $f_{12}$  and  $\phi_{12}$  as functions of  $q_{12}^z$  for  $(\tau_0, \Delta\tau) = (6.5, 0.65), (4.8, 2.4),$  and  $(3.2, 3.2)$  fm for the Heinz profile function, shown by solid, dashed, and dotted curves, respectively. See the text for the parameter values used.

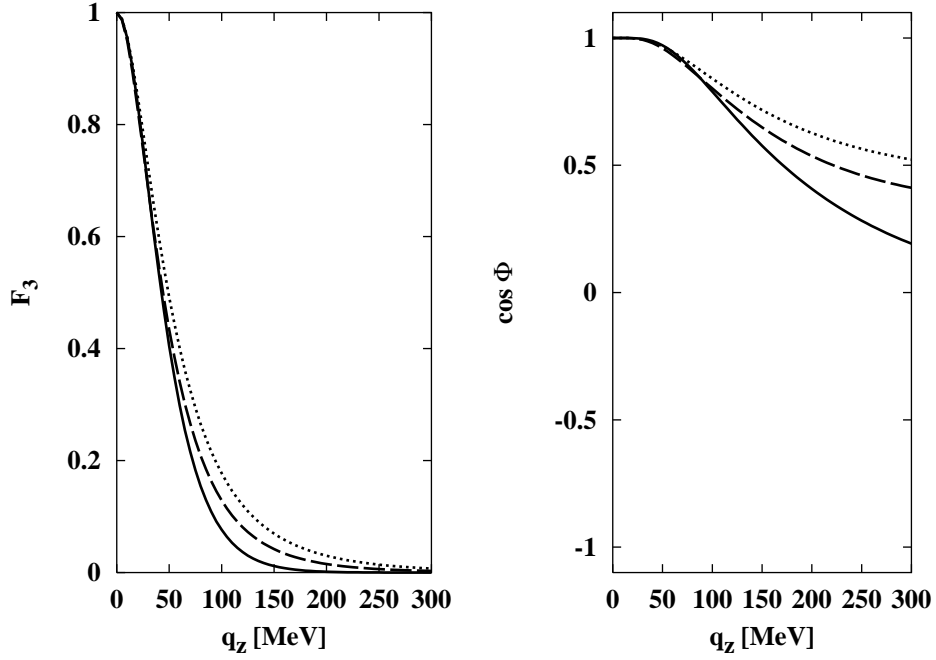


FIG. 15.  $\cos \Phi$  and  $F_3$  as functions of  $q_z$  for  $(\tau_0, \Delta\tau) = (6.5, 0.65), (4.8, 2.4),$  and  $(3.2, 3.2)$  fm for the Heinz profile function, shown by solid, dashed, and dotted curves, respectively. See the text for the parameter values used.

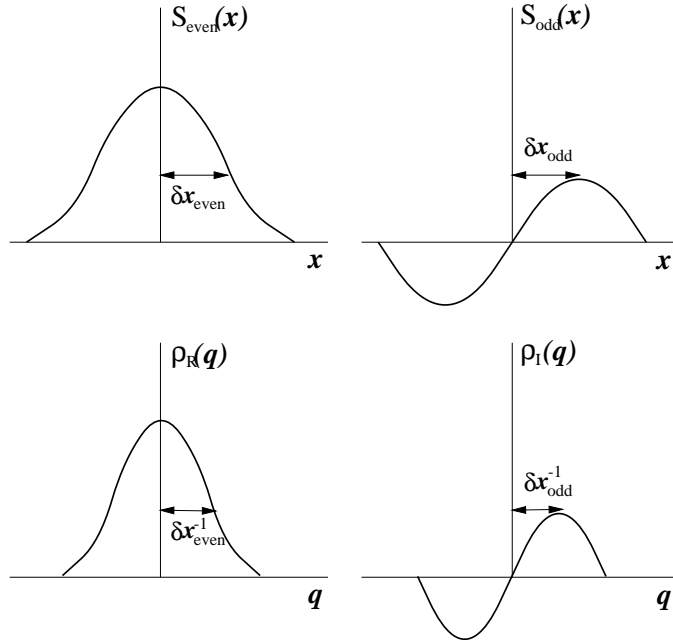


FIG. 16. Distances of typical scale over which  $S_{even}$  and  $S_{odd}$  vary.